Impact of Plasma Response on RMP ELM Suppression in DIII-D

A. Wingen[1], N.M. Ferraro[2], M.W. Shafer[1], E.A. Unterberg[1], T.E. Evans[2], D.L. Hillis[1], P.B. Snyder[2]

[1]*Oak Ridge National Laboratory, PO Box 2008, Oak Ridge, TN 37831, USA*

[2]*General Atomics, PO Box 85608, San Diego, CA 92186-5608, USA*

In this paper we will analyse several DIII-D discharges with different resonant and non-resonant plasma responses to applied resonant magnetic perturbations (RMPs) for edge-localized mode (ELM) suppression. We will show that the kink response strongly correlates with the edge current density profile and that discharges with stronger kink-response are closer to the peeling-ballooning stability limit and eventually cross into the unstable region, causing ELMs to reappear. All discharges have similar shaping and $1.59 \leq \beta_N \leq 2.46$. Although β_N varies between discharges, no correlation between the kink response and β_N or the pressure gradient is found here. Plasma response to externally applied RMPs has become increasingly relevant to tokamak research due to its impact on H-mode discharges. One particularly important effect is the mitigation or suppression of ELMs [1, 2, 3]. Many different physics effects have to be considered when calculating a self-consistent plasma response to applied fields, and various plasma parameters including dissipation and rotation impact the outcome. Here the M3D-C1 code [4], a resistive, two-fluid MHD code, is used to calculate the linear plasma response. Depending on plasma conditions, the plasma response can have various effects on the magnetic topology, such as screening/amplification of pitch-resonant field components (island response) relative to those in the applied spectrum, and amplification of non-pitch-resonant components (kink response); the latter introduces a corrugation of flux surfaces [5].

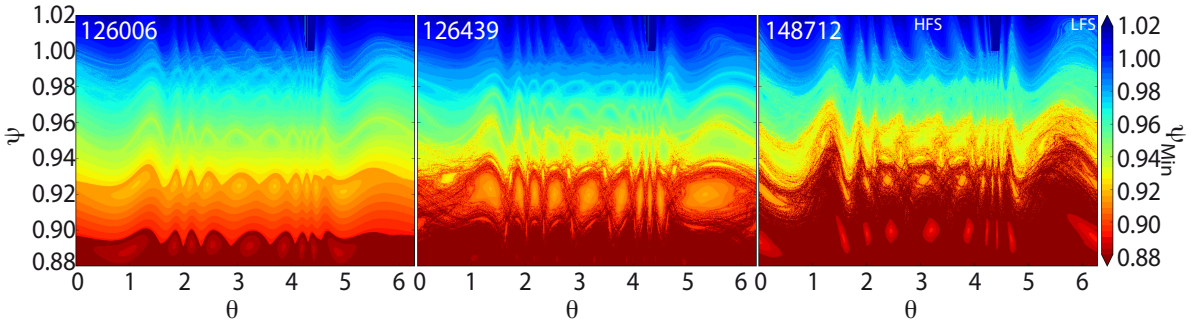

Figure 1: Magnetic topology in the poloidal cross-section at toroidal angle $\varphi = 262°$ for three discharges. The color represents contours of field line penetration depth ψ_{Min} in terms of unperturbed poloidal flux. Parameters (shot: B_t [T], I_p [MA], q_{95}, β_n) are: (126006: 1.92, 1.55, 3.52, 2.46), (126439: 2.14, 1.67, 3.58, 1.94), (148712: 2.01, 1.61, 3.37, 1.75).

Figure 1 shows the magnetic topology in DIII-D, with plasma response and the same 3 kA I-coil-like, pure $n = 3$ RMP applied, at the plasma edge in a poloidal cross-section, given by the

poloidal angle θ and the normalized poloidal flux ψ, for three different discharges. The color represents the field line penetration depth ψ_{Min}: at each grid point in the (θ, ψ) plane, a field line is launched and traced towards the inner and outer target, respectively, for a high number of toroidal turns or until it hits the vessel wall. The minimum of normalized flux, reached by the field line during the trace, is the penetration depth. Field lines on a closed magnetic surface all have the same unique penetration depth, so that contours of constant penetration depth agree with the magnetic topology. Stochastic regions on the other hand appear as fractals or large uniform areas. So the penetration depth represents the magnetic structure. Each discharge shows similar features in the magnetic topology, but with very different emphasis. In 126006 islands are very small due to screening of the pitch-resonant RMP field components, therefore there is very little stochasticity. Further, only a small amount of surface corrugation, called kinking, is observed. In 126439 there are small islands at the very edge, outside of $\psi = 0.94$, and the 10/3 island chain at about $\psi = 0.92$ is amplified; i.e. this island chain is larger than in the vacuum approximation, due to the plasma response of this pitch-resonant field component. Island overlap creates a stochastic layer around the 10/3 chain. The kinking appears larger than in 126006, but still moderate. The third case, 148712, shows predominantly a strong kinking as well as a strong pitch-resonant amplification of the 10/3 and 9/3 islands; further out the islands are again partially screened. The kinking is the dominant effect in this case though, since the remnant islands are forced to follow the corrugated surface structure. So, we observe that the kink response more and more dominates the magnetic structure in correlation with increasing parallel edge current density. Note that the island response is governed by rotation, independent from the kink response.

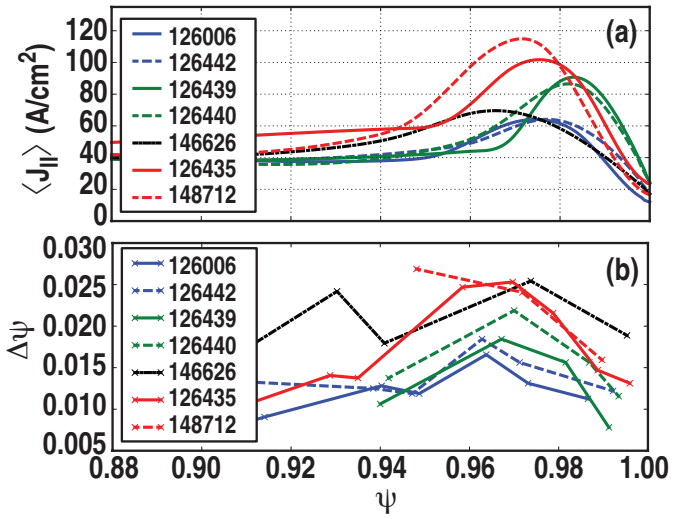

Figure 2: (a) Flux surface averaged parallel edge current density for various discharges. (b) Flux surface displacement, given by difference of maximum and minimum normalized poloidal flux of constant penetration depth contour lines in the magnetic edge topology for the same discharges as in (a).

In the following we focus on the kinking, which is caused by amplification of non-pitch-resonant RMP field components due to plasma response. We analysed a set of seven discharges and found a clear correlation between the flux surface averaged parallel edge current density $\langle j_{||} \rangle$ and the kinking of flux surfaces in the magnetic topology. The former is obtained through a kinetic

equilibrium reconstruction, including bootstrap current, while the latter is extracted from the simulated magnetic topology, like Fig. 1, by taking the difference $\Delta\psi$ between maximum and minimum ψ of the corrugated color contours in between island chains as long as the region is not stochastic. The findings are shown in Fig. 2. The upper figure shows the edge current density, while the lower shows the radial displacement of the surfaces (kink displacement). The color coding of the lines groups discharges with similar magnetic topology. The first group, blue lines, is represented by 126006 in Fig. 1, has a low edge current density and is characterized by small or no kinking, as shown in Fig. 2(lower). The second group, green lines, is represented by 126439, has a moderate edge current density and increased kinking. The third group, red lines, is represented by 148712, has the largest edge current density and also a strong kinking. Not only the order of the groups, but also the radial distribution of the kink displacements agree with the shape of the edge current density profiles, respectively. There is one further case, 146626, black line, which has a small to moderate edge current density, but larger displacements. This is due to a different q_{95} in 146626 of $q_{95} = 3.71$, compared to $q_{95} \approx 3.58$ in the 126-series and $q_{95} = 3.37$ in 148712, which moves the 11/3 islands further inwards, which is amplified here instead of partially screened, as in the other cases. The kink displacement is then superimposed with the amplified island envelope, which overestimates the black line in Fig 2.

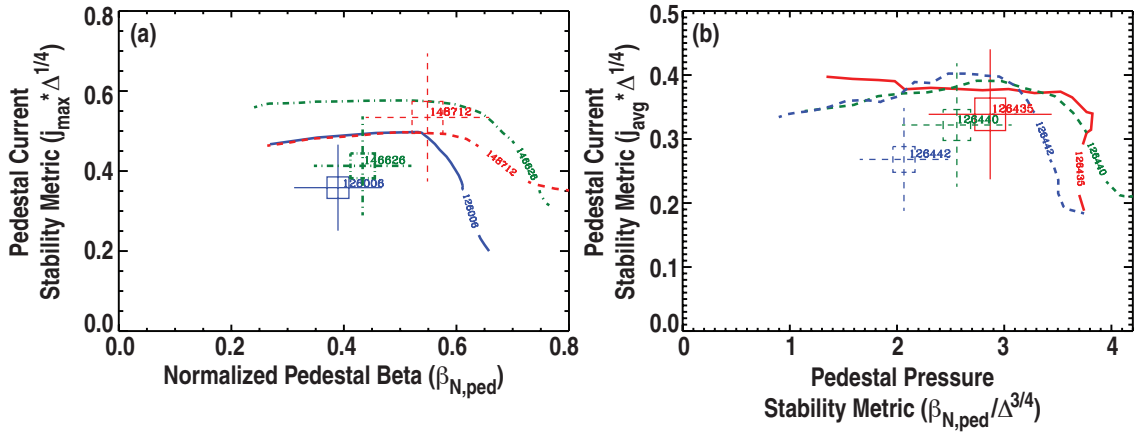

Figure 3: Peeling-ballooning stability diagrams for discharges 126006, 146626, 148712 (a) and 126435, 126440, 126442 (b). The crosses mark the operational points with error bars and the curves mark the respective stability boundaries ($\gamma/(\omega_{*,pi}/2) = 1$ contours). The color coding agrees with the color coding in Fig. 2. Note that the axes in the left and right figure are normalized differently.

Figure 3 shows an ELM stability analysis, using the ELITE code [6], for the discharges discussed in Fig 2 (same color and style here). The edge current is plotted versus the edge pressure. Both axes are normalized to make the discharges comparable and align the stability boundaries as best as possible; see Ref. [7] for details on the metrics. The lines are the $\gamma = \omega_{*,pi}/2$ contours with the peeling-ballooning instability growth-rate γ and the ion pressure diamagnetic frequency $\omega_{*,pi}$; they mark the onset of the instability. The crosses represent the operational points for each

discharge respectively, including error bars. As shown in Fig. 3, kink dominated discharges (red lines) are much closer to the stability boundary in peeling-ballooning-stability simulations than island dominated discharges (blue lines), which are well inside the stability limit. Discharges with moderate kink displacements (green lines) are located in between. This is consistent with discharges that have large kinking being more likely to show peeling ballooning instability in the presence of RMP, than discharges with less kinking.

Experimental observations are in agreement with the simulations. In the red cases ELMs are observed, while in the blue and green cases ELMs are fully suppressed by the applied RMP. Discharge 126435 (solid red line) shows ELM mitigation and not full suppression after the onset of the RMP phase. In 148712 the $n = 3$ RMP is phase-flipped 60° toroidally with a frequency of 5 Hz. After about 3100 ms into the discharge the ELMs return in one phase of the RMP, while the other phase remains suppressed. So, the discharge oscillates between ELM-free and ELMy.

For all cases, we compared simulations of the magnetic topology, which includes linear plasma response, as calculated by linear, resistive, 2-fluid MHD. It is found that the kink-response is strongly correlated to the parallel edge current density, but not to the pressure gradient, although this is not explicitly discussed here. The magnetic topology of discharges with low edge current density mainly shows islands, even with screening. With increasing edge current density the edge topology transitions to a kink dominated structure where islands are forced to follow the surface corrugation. A correlation between the kink-response and the reappearance of ELMs in the presence of RMPs is found. It could be speculated that experimentally minimizing the edge current density for a given pressure profile would improve RMP ELM control. ELITE simulations and experimental observation are in agreement with the findings.

This work was supported by the US Department of Energy under DE-AC05-00OR22725, DE-FC02-04ER54698 and DE-FG02-95ER54309.

References

[1] T. E. Evans *et al.*, Phys. Rev. Lett. **92**, 235003 (2004).

[2] Y. Liang *et al.*, Phys. Rev. Lett. **98**, 265004 (2007).

[3] W. Suttrop *et al.*, Phys. Rev. Lett. **106**, 225004 (2011).

[4] N. M. Ferraro, Phys Plasmas **19**, 056105 (2012).

[5] A. Wingen *et al.*, Nucl. Fusion **accepted** (2014).

[6] P. B. Snyder *et al.*, Phys Plasmas **9**, 2037 (2002).

[7] P. B. Snyder *et al.*, Nucl. Fusion **49**, 085035 (2009).